THE ASTROPHYSICAL JOURNAL, 415:734–749, 1993 October 1

THE RELATIVISTIC SOBOLEV METHOD APPLIED TO HOMOLOGOUSLY EXPANDING ATMOSPHERES

DAVID J. JEFFERY
Harvard-Smithsonian Center for Astrophysics MS-19, 60 Garden Street, Cambridge, MA 02138
Received 1992 April 20; accepted 1993 April 12

ABSTRACT

In this paper, a detailed application of the relativistic Sobolev method of Hutsemékers & Surdej (HS) to homologously expanding atmospheres (with supernovae as the only example in mind) is described. The expressions for the common-direction (CD) and common-point (CP) frequency surfaces for homologous expansion are derived. The CP frequency surfaces are necessary for interacting line effects and were not considered by HS. Other important expressions of the relativistic Sobolev method are presented and briefly discussed. The validities for supernovae of the stationarity approximation and the relativistic Sobolev method's neglect of advection are briefly discussed. Some demonstration spectra calculated using the relativistic and classical Sobolev methods for models in homologous expansion are presented and compared. For the analysis of supernova atmospheres with the highest velocities observed, the relativistic Sobolev method treatment yields a small, but significant, improvement over the classical Sobolev method treatment.

Subject headings: line: formation — radiative transfer — relativity — stars: atmospheres

1. INTRODUCTION

The well-known Sobolev method is an approximate radiative transfer technique introduced by Sobolev (1947) and extended by others (e.g., Castor 1970; Rybicki 1970; Lucy 1971; Rybicki & Hummer 1978, hereafter RH; Klein & Castor 1978; Olson 1982; Hummer & Rybicki 1985, 1992; Bartunov & Mozgovoi 1987; Puls & Hummer 1988; Jeffery 1988, 1989, 1990; Mazzali 1988, 1989, 1990; Hutsemékers & Surdej 1990, hereafter HS) which is used to calculate line radiative transfer in atmospheres with large velocity gradients. The classical Sobolev method relies on the first-order Doppler shift formula and is thus nonrelativistic. In this paper, it is assumed that the reader is familiar with the Sobolev method and the concepts of common-direction (CD) frequency surface (used for evaluating the flux emergent from an atmosphere), common-point (CP) frequency surface (used for evaluating the line source functions in an atmosphere with interacting line effects), resonance point and region, and Sobolev optical depth and escape probability. The paper of RH is a useful reference for the Sobolev method. The criterion for the Sobolev method's validity (except in the case of extremely strong lines; see Hummer & Rybicki 1992) is that the ratio (here called the velocity ratio) of the atmosphere's characteristic random velocity (i.e., the thermal velocity or perhaps a mean microturbulent velocity) to the velocity scale height (i.e., the velocity range over which temperature, density, and occupation numbers change by a factor of order 2) be small. For quantitative accuracy, the velocity ratio should be $\lesssim 0.1$ (Hamann 1981; Olson 1982; Natta & Beckwith 1986). (Note that Hamann's strictures on the Sobolev method's treatment of interacting line effects were made obsolete by Olson.) The Sobolev method has been useful for calculating synthetic spectra for stars with winds (e.g., Pauldrach, Puls, & Kudritzki 1986; Pauldrach 1987; Puls 1987) and supernovae (e.g., Branch et al. 1985; Jeffery & Branch 1990; Jeffery et al. 1992, hereafter JLK; Kirshner et al. 1993).

The Sobolev method is particularly suitable for supernovae. Supernova atmospheres have thermal velocities no larger than of order 10 km s^{-1} (except at early and almost never observed epochs) and microturbulent velocities are usually thought to be negligible. Supernova velocity scale heights in the photospheric epoch are $\sim 10^3$ km s^{-1}. Therefore, supernova velocity ratios are $\sim 10^{-2}$. The velocity field, called (uniform motion) homologous expansion, exhibited by supernovae after early, and almost never observed, epochs, is an especially simple case of general expansion. In homologous expansion, the radius of any matter element is given by

$$r = vt \,, \tag{1}$$

where v is the element's constant velocity and t is the time since all the elements were in one place. Supernovae enter homologous expansion when initial radii of matter elements and all forces acting on the matter elements become negligible. The classical CD and CP frequency surfaces for homologous expansion are planes perpendicular to the line of sight and spheres centered on resonance points (i.e., the common points of the CP frequency surfaces), respectively (see §§ 2 and 3). The classical Sobolev optical depth for homologous expansion is direction independent (see § 4). The simplicities of homologous expansion are, however, lost if ejecta velocities are so high that the classical treatment (including the use of the first-order Doppler shift formula) becomes inadequate. Typical supernova ejecta velocities, detected from line Doppler shifts, are of order 5000–15,000 km s^{-1}. Thus, relativistic corrections to the classical (i.e., first order) Doppler shifts are typically less than of order 5%. There are, however, observations revealing higher, and in a few cases much higher, supernova ejecta velocities. The blue edge of what is probably the P Cygni absorption of the Mg II resonance lines in an *IUE* spectrum of Type II supernova SN 1987A from day 1.658 after the explosion (Kirshner et al. 1987) suggests that there was ejecta moving at $\sim 40{,}000$ km s^{-1}. The blue edges of the Ca II H and K lines' P Cygni absorptions in premaximum spectra from Type Ia supernovae SN 1984A (Wegner & McMahan 1987; Branch 1987) and SN 1990N (Leibundgut et al. 1991; JLK) also suggest that there must be some ejecta at $\sim 40{,}000$ km s^{-1}. Even higher ejecta velocities may yet be detected in future observations. At

velocities of $\sim 30{,}000$ km s^{-1}, the classical Doppler shifts are in error by $\sim 10\%$ and a relativistically correct treatment of radiative transfer becomes desirable.

HS developed a relativistic Sobolov method intended for applications to objects with very high ejecta velocities such as broad absorption-line quasars and supernovae. A principal difference from the classical Sobolev method is that the relativistic CD and CP frequency surfaces do not have constant velocity components in the specifying directions of these surfaces; of course, the CD frequency surfaces still emit line radiation at a constant frequency in the frame of an observer at infinity and the CP frequency surfaces in the comoving frames of their common points. Because of this difference, it is better to refer to these surfaces as frequency surfaces following HS rather than to use the expression velocity surfaces used by, e.g., RH. HS did not consider relativistic CP frequency surfaces (and therefore interacting line effects) nor the case of homologous expansion at least as we define this case. Because of the high velocities in supernova ejecta, the lines in supernova atmospheres, especially blueward of 5000 Å, are almost always significantly interacting with other lines and interacting line effects cannot be ignored.

In this paper, a detailed application of the relativistic Sobolev method including interacting line effects to homologously expanding atmospheres (with supernovae as the only example in mind) is described. The expressions for the CD and CP frequency surfaces for homologous expansion are derived in §§ 2 and 3, respectively. We also discuss beam paths in the comoving frame in the CD and CP frequency surface cases. In § 4, other important expressions of the relativistic Sobolev method are presented and briefly discussed. The expressions assume that the velocity field of the atmosphere is spherically symmetric, but not that it is a homologous expansion velocity field or even a monotonic velocity field (see definition below). The expressions do not take account of advection. In § 5, we discuss for the case of supernovae the validities of making the stationarity approximation and of the relativistic Sobolev method's neglect of advection. In § 6, some demonstration spectra calculated using the relativistic and classical Sobolev methods for models in homologous expansion are presented and compared. Conclusions are given in § 7. The Appendix discusses the relativistic Sobolev method in the case of atmospheres in exponential expansion, a near relative of homologous expansion.

Before ending this introduction, there are a few further points we should discuss. Because this paper deals with quantities in both the comoving and observer frames, it is useful to recall the Lorentz transformations for these quantities. The subscript or superscript 0 will be used to denote comoving frame quantities. The relations for frequency and cosine of angle from the radial direction for a system with a spherically symmetric velocity field are

$$\nu_0 = \nu\gamma(1 - \mu\beta)\,, \quad \nu = \nu_0\,\gamma(1 + \mu_0\,\beta)\,, \tag{2}$$

$$\mu_0 = \frac{\mu - \beta}{1 - \mu\beta}\,, \quad \mu = \frac{\mu_0 + \beta}{1 + \mu_0\,\beta} \tag{3}$$

(e.g., Mihalas 1978, p. 495), where β is the radial velocity divided by c and

$$\gamma = \frac{1}{\sqrt{1 - \beta^2}}\,. \tag{4}$$

The azimuthal angle about the radial direction is the same in both frames. The relations for specific intensity, source function, and opacity are

$$\frac{I^0_{\nu_0}}{\nu_0^3} = \frac{I_\nu}{\nu^3}\,, \tag{5}$$

$$\frac{S^0_{\nu_0}}{\nu_0^3} = \frac{S_\nu}{\nu^3}\,, \tag{6}$$

$$\nu_0\,\chi^0_{\nu_0} = \nu\chi_\nu\,, \tag{7}$$

respectively (e.g., Mihalas 1978, pp. 495–496).

Homologous expansion is an example of what we will call a monotonic velocity field. We define a monotonic velocity field to be a velocity field in either general expansion or general contraction: i.e., a velocity field where matter is everywhere in either expansion or contraction. In such a velocity field, the velocity component along any possible beam path is either strictly increasing or decreasing. An example of a nonmonotonic velocity field can be a spherically symmetric decelerating outflow.

It should be emphasized that relativistic radiative transfer calculations for supernovae using techniques other than the Sobolev method are now common. First-order relativistic Monte Carlo calculations have been reported by Lucy (1987) and first-order relativistic comoving frame calculations by, e.g., Eastman & Kirshner (1989). Full relativistic comoving frame calculations have been done by Harkness (1991a, b; Wheeler & Harkness 1990) and by Hauschildt, Best, & Wehrse (1991). Comparisons of calculations with these techniques and the relativistic Sobolev method ought to be done; such comparisons are, however, beyond the scope of the present paper.

Since Monte Carlo and comoving frame techniques can be made more exact than the Sobolev method and are capable of treating low-velocity regimes as the Sobolev method is not, the reasons for the further use of the Sobolev method for supernovae ought to be mentioned. Sobolev method codes are simpler to develop and are less computationally demanding than the other techniques and so are more suitable for fast extensive analyses of supernova spectra. In detailed non-LTE calculations of supernova spectra, the Sobolev method provides a very useful means of calculating radiative transition rates (e.g., Eastman & Pinto 1993). The Sobolev method can be applied to aspherical systems (Jeffery 1987, 1988, 1989, 1990, 1991a, b), whereas the comoving frame formalism has not been generalized for these systems and Monte Carlo calculations for aspherical systems would be computationally very demanding. The Sobolev method offers a useful mental picture of radiative transfer. Given these reasons for using the Sobolev method, further improvement of supernova Sobolev calculations by making them relativistic seems worthwhile especially as the implementation of the relativistic effects turns out to be straightforward.

2. THE CD FREQUENCY SURFACES FOR HOMOLOGOUSLY EXPANDING ATMOSPHERES

Consider an atmosphere in homologous expansion and an atomic line with (comoving) line center frequency ν_0. Let there be a cylindrical coordinate system with symmetry axis along the line of sight and an impact parametere axis pendicular to the symmetry axis and intersecting it at the expansion center. We use z as the symmetry axis coordinate with positive z in the direction of the observer and p as the impact parameter coordi-

nate. We will measure velocity in units of c, and therefore use β rather than v as the velocity symbol. The CD frequency formulae for the line will be given in terms of velocities; spatial distances can be obtained by multiplying the velocities by the appropriate time. In order to obtain these formulae, consider a point with radial velocity β, z-axis velocity β_z and impact parameter velocity β_p. These velocities are related by

$$\beta_z = \mu\beta\,, \quad \beta = \sqrt{\beta_z^2 + \beta_p^2}\,. \tag{8}$$

Let

$$d = \frac{v}{v_0}\,, \quad \delta = d - 1 = \frac{v}{v_0} - 1\,. \tag{9}$$

Substituting from equations (8) and (9) into the first expression of equation (2) and solving for β_z gives

$$\beta_z = \beta_{z\pm} = \frac{d^2 \pm \sqrt{1 - (d^2 + 1)\beta_p^2}}{d^2 + 1}\,. \tag{10}$$

The two solutions for β_z are the relativistic formulae for the CD frequency surfaces. The lower case solution is the classical analog solution. The upper case solution is a purely relativistic solution.

The surface defined by equation (10) is in fact an axisymmetric ellipsoid with center at the velocity point $(\beta_p, \beta_z) = [0, d^2/(d^2 + 1)]$, and semimajor axis, semiminor axis, and eccentricity

$$\frac{1}{\sqrt{d^2 + 1}}\,, \quad \frac{1}{d^2 + 1}\,, \quad \frac{d}{\sqrt{d^2 + 1}}\,, \tag{11}$$

respectively. When the discriminant of equation (10) is zero (i.e., when β_p equals the semimajor axis), the two solutions for β_z reduce to one solution and we have a limiting CD frequency surface velocity point. For this limiting velocity point, we have the limiting velocity

$$\beta_{\rm lim} = \frac{\sqrt{d^4 + d^2 + 1}}{d^2 + 1}\,. \tag{12}$$

The behavior of $\beta_{\rm lim}$ as a function of d is of interest. For both $d = 0$ (redshift to zero-frequency case) and $d = \infty$ (blueshift to infinite frequency case), $\beta_{\rm lim} = 1$; thus, the velocity at the limiting impact parameter position is the velocity of light. For d between 0 and ∞, $\beta_{\rm lim}$ has one stationary point, a minimum for $d = 1$ where $\beta_{\rm lim} = (3)^{1/2}/2$. The behavior of the $\beta_\pm$ function (i.e., of $[\beta_{z\pm}^2 + \beta_p^2]^{1/2}$) with constant d is monotonic decreasing with β_p for the upper case and monotonic increasing with β_p for the lower case. Thus, for any value of d including $d = 0$,

$$\beta_- \le \beta_{\rm lim} \le \beta_+\,. \tag{13}$$

It follows that upper case solution for the CD frequency surface will be physically relevant only for a homologously expanding atmosphere where matter is moving at radial velocities greater than $(3)^{1/2}/2$ (in units of c). To present knowledge, there are no astrophysical atmospheres exhibiting physical velocities at all close to $(3)^{1/2}/2$. Consequently, the upper case solutions are currently only interesting formalism.

To second order in small δ and β_p, the classical analog solution for the CD frequency surface is

$$\beta_{z-}^{2d} = \delta - \tfrac{1}{2}\delta^2 + \tfrac{1}{2}\beta_p^2\,. \tag{14}$$

The first-order classical analog solution,

$$\beta_{z-}^{1st} = \delta = d - 1 = \frac{v}{v_0} - 1\,, \tag{15}$$

is, of course, the classical solution itself; one can see that the classical CD frequency surfaces are planes perpendicular to the line of sight.

Figure 1 displays the behavior of the CD frequency surfaces for several values of d. For $d = 0$, the two solutions form a sphere of radius 1. As d increases, the ellipsoid formed by the two solutions shifts toward higher β_z values, contracts, and increases in eccentricity. For $d = \infty$, the closed curve formed by the two solutions contracts to a point with $\beta_z = 1$, $\beta_p = 0$, and $\beta = 1$. The upper case solution for $\beta_p = 0$ always has $\beta_z = \beta = 1$. Naturally, the solutions are unphysical when they have $\beta = 1$: i.e., when they correspond to a frame moving at the velocity of light. In the classical case, redshifted and blueshifted line photons emitted by the atmosphere can only come from the $\beta_z < 0$ and $\beta_z > 0$ regions of the atmosphere, respectively (see eq. [15]). Figure 1 shows that in the relativistic case redshifted photons can come from the $\beta_z > 0$ region for sufficiently large β_p. Noting, however, that

$$d = \frac{\sqrt{1 - \beta^2}}{1 - \beta_z} < 1 \quad \text{for} \quad \beta_z < 0 \tag{16}$$

(see eqs. [2], [4], [8], and [9]), it follows that all line photons coming from the $\beta_z < 0$ region are redshifted, and thus (and just as in the classical case) blueshifted line photons can only come from the $\beta_z > 0$ region. Figure 1 suggests that the closed CD curves for different d values never intersect. This suggestion is easily confirmed. The upper and lower cases of equation (10) are strictly decreasing and increasing functions of d, respectively, for $d > 0$, except for the upper case solution for $\beta_p = 0$ which is 1 for all d and which can be ignored for this argument. Thus, along any impact parameter β_p, one upper

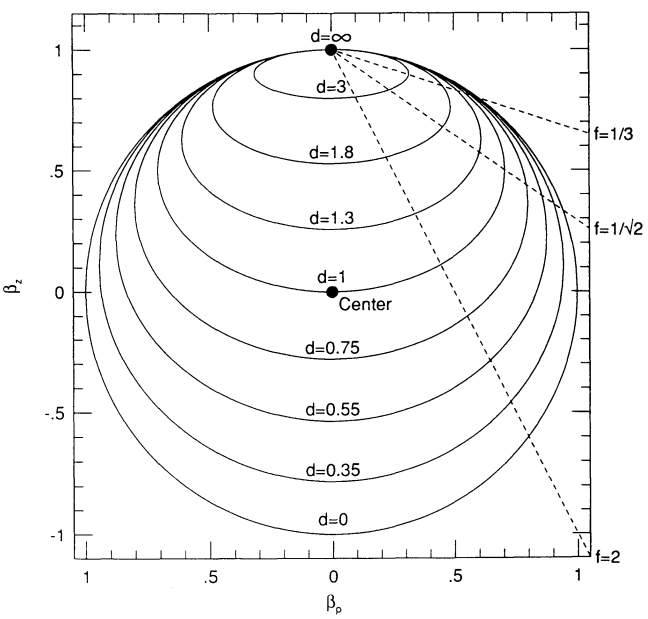

FIG. 1.—The homologous expansion case CD frequency surfaces for several values of $d = v/v_0$ are marked by solid lines. The expansion center and the point solution for the $d = \infty$ case are marked by dots. Beam paths for several f values are marked by dashed lines.

(lower) case solution can never intersect another upper (lower) case solution. Since along any impact parameter β_p, the lowest upper case solution β_z value and the highest lower case solution β_z value are the same β_z value and in both cases the β_z values are obtained for the same limiting d value given by

$$d_{\rm lim} = \sqrt{\beta_p^{-2} - 1}\,, \tag{17}$$

it is clear that the closed CD curves of constant d never intersect at all. The existence of $d_{\rm lim}$ means, of course, that lines cannot give rise to arbitrarily large shifts for specified $\beta_p > 0$.

Consider a beam propagating in the z-direction that at time t_1 is located at point $(p_1, z_1) = (\beta_{p,1}\, t_1, \beta_{z,1}, t_1)$, where $\beta_{p,1} > 0$. As time passes, the impact parameter of the beam stays constant at p_1, but the impact parameter velocity decreases according to

$$\beta_p = \frac{p_1}{ct}\,. \tag{18}$$

The z coordinate increases according to

$$z = c(t - t_1) + z_1\,. \tag{19}$$

It follows from equations (18) and (19) that

$$\beta_z = 1 - f\beta_p\,, \tag{20}$$

where we define

$$f = \frac{1 - \beta_{z,1}}{\beta_{p,1}}\,. \tag{21}$$

Thus, a z-directed beam in the comoving frame follows a straight line path where $\beta_z = 1$ when $\beta_p = 0$: i.e., when $t = \infty$. Beams paths for several f values are marked by dashed lines in Figure 1. From Figure 1, it appears unlikely that a beam can intersect the CD frequency surfaces for line (i.e., for a given d value) more than once not counting the always present unphysical intersection at the velocity point (0, 1). If one substitutes the solutions for the CD frequency surfaces (see eq. [10]) into equation (20), one obtains a single solution (aside from the unphysical solution $[\beta_p, \beta_z] = [0, 1]$) for the velocity point of intersection between the beam and the CD frequency surfaces:

$$(\beta_p, \beta_z) = \left[\frac{2f}{(d^2 + 1)f^2 + 1}, \frac{(d^2 - 1)f^2 + 1}{(d^2 + 1)f^2 + 1}\right]. \tag{22}$$

For $f < 1/(d^2 + 1)^{1/2}$, the beam intersects the upper case solution CD frequency surface and for $f > 1/(d^2 + 1)^{1/2}$, the lower case solution CD frequency surface. For $f = 1/(d^2 + 1)^{1/2}$, the beam, of course, intersects the limiting CD frequency surface velocity point. If $\beta_p = 0$ for a beam at a finite time, then $\beta_p = 0$ always and the beam is collinear with the z-axis; such a beam obeys equation (19), of course, and only intersects the upper case CD frequency surface solutions at the velocity point (0, 1).

Because only one physically relevant intersection of a z-directed beam and the CD frequency surfaces for a line can occur, there is no direct remote radiative coupling of a line to itself in homologously expanding atmospheres. In § 3, we will demonstrate that propagating photons always become redder in the homologous expansion comoving frame, and thus remote self-coupling mediated by a second line is not possible either. The monotonic shifting of photon frequency also occurs in all monotonic velocity fields in the classical limit (because the first-order Doppler formula applies) where remote self-coupling is likewise not possible. Atmospheres in exponential expansion (like homologous expansion a form of general expansion) with very high velocities can exhibit a relativistic remote self-coupling as pointed out by HS (see the Appendix). A nonrelativistic remote self-coupling can occur, of course, in atmospheres with nonmonotonic velocity fields where there are remote matter elements that are at rest with respect to each other. Such atmospheres are discussed by RH (see also § 4).

In calculating the formal Sobolev solution for the emergent flux from an atmosphere, the usual procedure is to add up the contributions to a z-directed beam from CD frequency surfaces and any continuum sources proceeding either forward or backward along the beam path. The beam may end on the farthest CD frequency surface being considered or on an opaque source of continuum radiation, usually a central radiating spherical core representing either a photosphere or a thermalization layer. Since the beams travel along straight lines in the comoving frame, dealing with occultation due to a core is straightforward. In § 4, the expressions for frequency surface contributions to a beam are presented. After calculating the flux in a beam, one integrates over all beams being emitted to get the net flux. For homologous expansion, equation (22) provides the locations of the points where a beam for a specified f parameter intersects the CD frequency surfaces. For example, if proceeding backward along a beam, one evaluates equation (22) for progressively bluer lines: i.e., progressively larger line center frequencies ν_0 or progressively smaller d values. One is also evaluating the contributions from the CD frequency surface at progressively earlier times as one proceeds backward along the beam. It is straightforward to show that no beams emitted by a core can interact with the upper case solution CD frequency surfaces, except that if the core is large enough to intersect upper case solution CD frequency surfaces, then interaction is possible at the points of intersection. Line and continuum photons emitted in the atmosphere and, as Figure 1 suggests, beams entering the atmosphere from other regions of space can interact with the upper case solution CD frequency surfaces.

One must do the integration over all beams for the net flux as an integration over a physical area in order to obtain the net flux in the proper units. For example, one may chose to integrate over the plane that is perpendicular to the line of sight and tangent to the outermost physical shell of the atmosphere. Let this shell have velocity $\beta_{\rm max}$. Say one does this integration at time t. The observer will see this flux at time

$$t_{\rm obs*} = t + t_C - t_{\rm max}\,, \tag{23}$$

where t_C is the light travel time from the expansion center to the observer and $t_{\rm max} = \beta_{\rm max} t$ is the light travel time from the expansion center to the outermost shell at time t. The observer's epoch is, of course, defined as $t_{\rm obs} = t_{\rm obs*} - t_C$. For a synthetic spectrum calculation, one usually specifies $t_{\rm obs}$ and obtains t from

$$t = \frac{t_{\rm obs}}{1 - \beta_{\rm max}}\,. \tag{24}$$

In a time-dependent calculation, clearly all atomic conditions must be specified as functions of time. For time-independent calculation (i.e., one making the stationarity approximation), one must choose an appropriate characteristic time. $t_{\rm ch}$, for these atomic conditions. In the case of supernovae, much of the

spectrum formation will occur relatively close to the expansion center or close to the plane perdendicular to the line of sight running the expansion center. Moreover, both matter nearer and farther than the expansion center are important for P Cygni profile formation. Therefore, the obvious choice for the characteristic time for supernovae is

$$t_{ch} = t - t_{max} = t_{obs} . \tag{25}$$

In § 5, we discuss the validity of time-independent supernova Sobolev method calculations.

3. THE CP FREQUENCY SURFACES FOR HOMOLOGOUSLY EXPANDING ATMOSPHERES

In order to find the homologous expansion case formulae for the CP frequency surfaces, consider a reasonance point P_1, a local line (i.e., a line at point P_1) with line center frequency ν_1^0, and a remote line (i.e., a line not at point P_1 in general) with line center frequency ν_2^0. The set of points from which a photon flow can occur from the remote line to the local line at P_1 constitutes a CP frequency surface for P_1; P_1 is the common point of this CP frequency surface. Consider a resonance point P_2 for the remote line located on this CP frequency surface. We will think of P_1 and P_2 as points attached to matter elements sharing in the homologous expansion. The diagram in Figure 2 shows the relevant quantities and geometry in the observer frame. Using equation (1), we know that

$$\beta_1 = \frac{r_1}{ct_1} , \quad \beta_2 = \frac{r_2}{ct_2} , \tag{26}$$

where t_2 and t_1 are the times when a photon traveling from P_2 to P_1 is at P_2 and at P_1, respectively. To specify the CP frequency surface, we need to find expressions in terms of β_1, μ_1, and ν_1^0 and ν_2^0 for β_2, μ_2, μ_C, μ_{1*} (see below), and $\Delta\beta$, the geometrical velocity difference between points P_1 and P_2 at one instant in time.

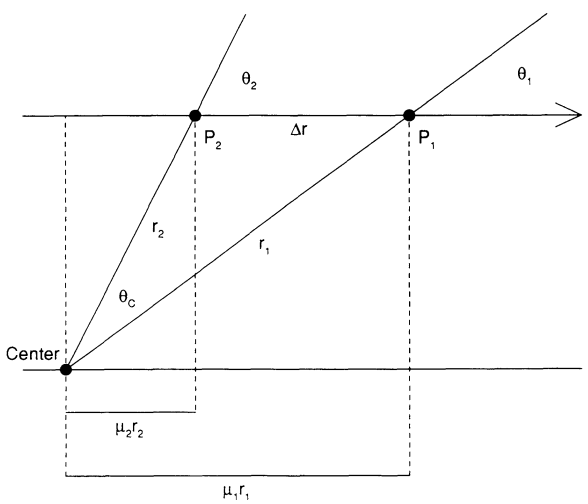

FIG. 2.—The relevant quantities and geometry in the observer frame needed to derive the formulae for the homologous expansion case CP frequency surfaces. The expansion center and the two resonance points are marked by dots. The line connecting the two resonance points is the observer-frame beam path between them. The arrow shows the direction of photon propagation.

Geometry provides us with the expressions

$$r_2 = \sqrt{r_1^2 + \Delta r^2 - 2r_1\Delta r\mu_1} , \tag{27}$$

$$r_1 = \mu_C r_2 + \mu_1 \Delta r , \tag{28}$$

$$\Delta r = \mu_1 r_1 - \mu_2 r_2 , \tag{29}$$

and physics with the expression

$$\Delta r = c(t_1 - t_2) . \tag{30}$$

We define

$$x = \frac{t_1}{t_2} . \tag{31}$$

Using these expressions, it is straightforward to obtain

$$\beta_2 = \sqrt{1 - 2x(1 - \mu_1\beta_1) + x^2(1 + \beta_1^2 - 2\mu_1\beta_1)} , \tag{32}$$

$$x = \frac{1 - \mu_2\beta_2}{1 - \mu_1\beta_1} , \tag{33}$$

$$\mu_2 = \frac{1 - x(1 - \mu_1\beta_1)}{\beta_2} , \tag{34}$$

$$\mu_C = \frac{x\beta_1 - (x - 1)\mu_1}{\beta_2} . \tag{35}$$

Then using the Law of Cosines and substituting as necessary gives

$$\Delta\beta = \sqrt{\beta_1^2 + \beta_2^2 - 2\beta_1\beta_2\mu_C} \tag{36a}$$

$$= (x - 1)\sqrt{1 + \beta_1^2 - 2\mu_1\beta_1} . \tag{36b}$$

Note that $\Delta\beta$ is a physical velocity only in the classical limit. We must now find an expression for x.

For the two lines to be radiatively coupled,

$$\frac{\nu_1^0}{\gamma_1(1 - \mu_1\beta_1)} = \frac{\nu_2^0}{\gamma_2(1 - \mu_2\beta_2)} \tag{37}$$

(see eq. [2]). Let

$$d_{12} = \frac{\nu_2^0}{\nu_1^0} , \quad \delta_{12} = d_{12} - 1 . \tag{38}$$

Using the expression for d_{12}, equation (33) for x, and equation (37), we obtain

$$x = \frac{d_{12}\gamma_1}{\gamma_2} = \frac{d_{12}\sqrt{1 - \beta_2^2}}{\sqrt{1 - \beta_1^2}} . \tag{39}$$

Substituting for β_2 from equation (32) and solving for x yields

$$x = \frac{2d_{12}^2(1 - \mu_1\beta_1)}{d_{12}^2(1 + \beta_1^2 - 2\mu_1\beta_1) + (1 - \beta_1^2)} . \tag{40}$$

We also have

$$x - 1 = \frac{(d_{12}^2 - 1)(1 - \beta_1^2)}{d_{12}^2(1 + \beta_1^2 - 2\mu_1\beta_1) + (1 - \beta_1^2)} . \tag{41}$$

Since $x - 1 \geq 0$ always, it follows from equation (41) that $d_{12} \geq 1$ always. Thus, propagating photons always get redder in the comoving frame and photon flow must always be from a bluer to a redder line. Remote self-coupling is not possible, but locally self-coupling is allowed, of course, for $d_{12} = 1$. The CP

frequency surfaces for exponential expansion cases, however, do allow remote self-coupling as we show in the Appendix. From equation (41), it is straightforward to show that $x - 1$ and therefore $\Delta\beta$ increase monotonically with d_{12}.

Given the expressions for x and $x - 1$, we can calculate β_2, μ_2, μ_C, and $\Delta\beta$. The CP frequency surface itself is obtained from the expressions for β_2 and μ_C. The cosine μ_2 is needed for the radiative transfer on the CP frequency surface (see § 4). The $\Delta\beta$ could be used to locate the CP surface if we knew μ_1 in terms of the analogous cosine for the geometry where the points P_1 and P_2 are considered at one instant in time. We denote this cosine by μ_{1*}. From the Law of Cosines we have

$$\beta_2 = \sqrt{\beta_1^2 + \Delta\beta^2 - 2\beta_1\Delta\beta\mu_{1*}} \,. \tag{42}$$

Using the expressions for β_2, $\Delta\beta$, and $x - 1$, we find

$$\mu_{1*} = \frac{\mu_1 - \beta_1}{\sqrt{1 + \beta_1^2 - 2\mu_1\beta_1}} \,. \tag{43}$$

It should be clear that μ_{1*} is not defined when $\Delta\beta = 0$ (i.e., when $d_{12} = 1$). Note that μ_{1*} is not the same as μ_1^0 (the physical comoving counterpart to μ_1; see eq. [3]); however, μ_{1*} $\mu_1^0 = \pm 1$ when $\mu_1 = \pm 1$, and μ_{1*} and μ_1^0 do agree to first-order in small β_1. It is easy to show that $\mu_{1*} \leq \mu_1$ always and that the equality holds only for $\mu_1 = \pm 1$. Inverting equation (43), we get

$$\mu_1 = \mu_{1*}\sqrt{1 - \beta_1^2(1 - \mu_{1*}^2)} + \beta_1(1 - \mu_{1*}^2) \,. \tag{44}$$

Using this expression we can now calculate $\Delta\beta$ as a function of μ_{1*}.

There is an interesting consequence to the fact that μ_{1*} and therefore θ_{1*} are independent of x and d_{12}. From the Law of Sines, we find that

$$\beta_2 \sin\theta_{2*} = \beta_1 \sin\theta_{1*} \,, \tag{45}$$

where θ_{2*} is the angle analogous to θ_2, but for the geometry where the points P_1 and P_2 are considered at one instant in time. Clearly, $\beta_2 \sin\theta_{2*}$ is also independent of x and d_{12}, and thus beams incident on P_1 must follow straight line paths in the comoving frame as well as in the observer frame. Since P_1 is an arbitrary point, all beams follow straight line paths in the comoving frame. This result also follows from our demonstration in § 2 that beams moving in the z-direction in the observer frame move along straight lines in the comoving frame, since any direction can be taken as the z-direction. Since the beams follow straight line paths in the comoving frame, the effective cosine of half the angle subtended by a central spherical core is

$$\mu_{1*\,\mathrm{core}} = \sqrt{1 - (\beta_{\mathrm{core}}/\beta_1)^2} \,, \tag{46}$$

where β_{core} is the core radial velocity.

Using equations (36) and (41), we find

$$\Delta\beta = \frac{(d_{12}^2 - 1)(1 - \beta_1^2)\sqrt{1 + \beta_1^2 - 2\mu_1\beta_1}}{d_{12}^2(1 + \beta_1^2 - 2\mu_1\beta_1) + (1 - \beta_1^2)} \,. \tag{47}$$

We can use equation (44) to make $\Delta\beta$ a function of μ_{1*} rather than μ_1. The CP frequency surface specified by equation (47) is axisymmetric, of course, but not an axisymmetric ellipsoid. The expressions for $\Delta\beta$ to third, second, and first order in small δ_{12} and β_1 are

$$\Delta\beta^{3\mathrm{d}} = \delta_{12}[1 - \tfrac{1}{2}\delta_{12} + \mu_1\beta_1\delta_{12} - \tfrac{1}{2}\beta_1^2(1 + \mu_1^2)] \,, \tag{48}$$

$$\Delta\beta^{2\mathrm{d}} = \delta_{12}(1 - \tfrac{1}{2}\delta_{12}) \,, \tag{49}$$

$$\Delta\beta^{1\mathrm{st}} = \delta_{12} = d_{12} - 1 = \frac{v_2^0}{v_1^0} - 1 \,, \tag{50}$$

respectively. The first-order solution is the expression for the classical CP frequency surface: i.e., a sphere centered on the common point. It is interesting to note that the spherical CP frequency surface is maintained to second order.

Figure 3 displays the behavior of the CP frequency surfaces for β_1 values 0.1 and 0.9, and δ_{12} values 0.1, 0.3, 1, 2, 5, and ∞. For $\beta_1 = 0.1$ and small δ_{12}, the CP frequency surface is nearly a sphere centered on the common point. As δ_{12} increases, the CP frequency surface distorts slightly and becomes a sphere of radius 1 centered on the expansion center for $\delta_{12} = \infty$. For $\beta_1 = 0.9$, the CP surface is oval-shaped for small δ_{12} and becomes a sphere of radius 1 centered on the expansion center for $\delta_{12} = \infty$.

To evaluate the line source function at a resonance point, one sums all the contributions to a beam incident on the point from the CP frequency surfaces and any continuum radiation sources, and then integrates over all angle. In § 4, the expressions for frequency surface contributions to a beam and for the relativistic line source function are presented.

4. RELATIVISTIC SOBOLEV METHOD FORMALISM

For reference, we present and briefly discuss in this section the relativistic Sobolev method expressions for resonance region line optical depth, width, and escape probability, the formal solution for radiative transfer through frequency surfaces (which is exactly as in the classical case), and the line

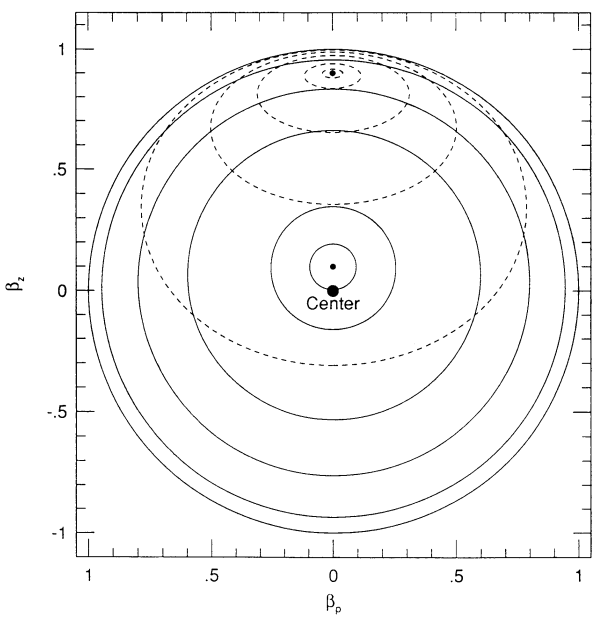

FIG. 3.—The homologous expansion case CP frequency surfaces for β_1 values 0.1 and 0.9, and δ_{12} values 0.1, 0.3, 1, 2, 5, and ∞. The two common points are marked by small dots and the expansion center by a large dot. The CP frequency surfaces for the $\beta_1 = 0.1$ and $\beta_1 = 0.9$ common points are drawn with solid and dashed lines, respectively. The CP frequency surfaces get monotonically larger as δ_{12} increases. The CP frequency surfaces for $\delta_{12} = \infty$ overlap exactly and are spheres of radius 1 centered on the expansion center.

source function. The derivations of these expressions are given by HS or follow directly from HS and classical Sobolev method presentations (e.g., RH and Jeffery & Branch 1990). The expressions assume that the velocity field of the atmosphere is spherically symmetric, but not that it is a homologous expansion or a monotonic velocity field. Additionally, the expressions assume (just as for the classical Sobolev method) that advection can be neglected; this assumption is discussed in § 5 for the case of supernovae. For the line source function expression, complete redistribution (CRD) in frequency and angle in the comoving frame is assumed; the analogous assumption is usually made for the classical Sobolev method where, of course, there is no distinction between comoving and observer frame quantities, except for frequency. A discussion is given of how the assumption of CRD in angle can be dispensed with for a certain kind of line scattering.

The expression for the relativistic Sobolev optical depth of a resonance region centered at a point P is given by

$$\tau = \frac{\alpha^0}{\nu_P^0} \frac{(1-\mu\beta)^2}{\gamma|\,\mu(\mu-\beta)\partial\beta/\partial r + (1-\mu^2)(1-\beta^2)\beta/r\,|}\,, \tag{51}$$

where ν_P^0 is the comoving line center frequency for a line for which P is a resonance point, α^0 is the comoving frame integrated line opacity at P, and β and $\partial\beta/\partial r$ are evaluated at P. The beams that will interact with the line at P must have observer frame frequencies ν satisfying $\nu_P^0 = \nu\gamma(1-\mu\beta)$. In the classical limit,

$$\begin{aligned}\tau = \tau^{1\mathrm{st}} &= \frac{\alpha^0}{\nu_P^0}\left|\frac{\partial(\mu\beta)}{\partial s}\right|^{-1} \\ &= \frac{\alpha^0}{\nu_P^0}\frac{1}{|\,\mu^2(\partial\beta/\partial r) + (1-\mu^2)\beta/r\,|}\,,\end{aligned} \tag{52}$$

where $\tau^{1\mathrm{st}}$ is, of course, the classical Sobolev optical depth (e.g., RH) and s is an observer frame beam path coordinate for a beam path through P in the direction determined by μ with $s = 0$ at P.

For homologous expansion,

$$\frac{\partial\beta}{\partial r} = \frac{\beta}{r} = \frac{1}{ct}\,, \tag{53}$$

and thus

$$\tau = \tau_{\mathrm{hom}} = \frac{\alpha^0 ct}{\nu_P^0}\frac{(1-\mu\beta)^2}{\gamma|\,\mu(\mu-\beta) + (1-\mu^2)(1-\beta^2)|}\,. \tag{54}$$

To second order in β, the homologous expansion Sobolev optical depth is given by

$$\tau = \tau_{\mathrm{hom}}^{2\mathrm{d}} = \frac{\alpha^0 ct}{\nu_P^0}(1-\mu\beta) = \tau_{\mathrm{hom}}^{1\mathrm{st}}(1-\mu\beta)\,, \tag{55}$$

where $\tau_{\mathrm{hom}}^{1\mathrm{st}}$ is the classical homologous expansion Sobolev optical depth. Clearly, the second-order correction to the classical homologous expansion Sobolev optical depth will tend to enhance outward transmission relative to inward transmission. The classical homologous expansion Sobolev optical depth is direction-independent.

The appropriate comoving frame frequency profile for a line in astrophysical contexts is usually a normalized Voigt function (e.g., Mihalas 1978, pp. 279–281). The Voigt function has a Gaussian core with a maximum at the line center frequency (here labeled ν_P^0) and becomes a Lorentzian function in the wings. The Gaussian core is due to the thermal velocity field and perhaps a microturbulent velocity field. When the Lorentzian wings are insignificant, the Voigt function becomes nearly zero when ν_0 differs from ν_P^0 by more than a few times the Gaussian width $\Delta\nu_{\mathrm{Ga}}^0$ which by the usual stellar atmospheres convention is $2^{1/2}$ times the Gaussian standard deviation. The Lorentzian wings will only become significant for very strong lines with Sobolev optical depths of order 10^3 or larger (e.g., Hummer & Rybicki 1992). If the thermal velocity field alone determines the Gaussian core, then the Gaussian width is the thermal frequency width and is given by

$$\Delta\nu_{\mathrm{Ga}}^0 = \Delta\nu_{\mathrm{th}}^0 = \nu_P^0\frac{v_{\mathrm{th}}^0}{c} = \frac{\nu_P^0\sqrt{2kT/m}}{c}\,, \tag{56}$$

where $\Delta\nu_{\mathrm{th}}^0$ is the thermal frequency width and v_{th}^0 is the thermal velocity; i.e., the most probable thermal speed or the thermal velocity width (e.g., Mihalas 1978, p. 110).

The observer frame resonance region (characteristic) width l_{res} is defined to be the spatial counterpart of the line Gaussian (frequency) width $\Delta\nu_{\mathrm{Ga}}^0$. The expression for l_{res} is

$$\begin{aligned}l_{\mathrm{res}} &= \frac{\Delta\nu_{\mathrm{Ga}}^0}{\nu|\,\partial/\partial s[\gamma(1-\mu\beta)]\,|} \\ &= \frac{\Delta\nu_{\mathrm{Ga}}^0}{\nu_P^0}\frac{(1-\mu\beta)}{\gamma^2|\,\mu(\mu-\beta)\partial\beta/\partial r + (1-\mu^2)(1-\beta^2)\beta/r\,|}\,,\end{aligned} \tag{57}$$

where $\Delta\nu_{\mathrm{Ga}}^0$, β, and $\partial\beta/\partial r$ have been evaluated at P. For homologous expansion,

$$\begin{aligned}l_{\mathrm{res}} &= l_{\mathrm{res\ hom}} \\ &= \frac{\Delta\nu_{\mathrm{Ga}}^0 ct}{\nu_P^0}\frac{(1-\mu\beta)}{\gamma^2|\,\mu(\mu-\beta) + (1-\mu^2)(1-\beta^2)|}\,.\end{aligned} \tag{58}$$

Note that if the Gaussian core of the line profile is determined by the thermal velocity field, then

$$\frac{\Delta\nu_{\mathrm{Ga}}^0 ct}{\nu_P^0} = v_{\mathrm{th}}^0 t \tag{59}$$

(see eq. [56]). The resonance region width can also be considered as the observer frame characteristic width of the CD or CP frequency surface on which the resonance point lies. Note that the resonance region can have an effective size scale that is much larger than the defined resonance region width if the Lorentzian wings of the line are not negligible.

The formal Sobolev solution for the radiative transfer of a beam through a single frequency surface in the limits of s (the beam path coordinate) going to effective negative and positive infinity relative to the frequency surface is

$$I_\nu = \begin{cases} I_\nu^{-\infty} & \text{for } s \to -\infty\,; \\ I_\nu^{-\infty}e^{-\tau} + S_\nu(1-e^{-\tau}) & \text{for } s \to \infty\,; \end{cases} \tag{60}$$

where $I_\nu^{-\infty}$ is beam intensity well before the frequency surface and S_ν is the observer frame line source function evaluated at the center of the frequency surface (i.e., at $s = 0$). This expression can be immediately generalized to the multiple line interaction case by considering all lines as effectively infinitely far apart: i.e., as not having overlapping resonance regions. The generalized expression is

$$I_\nu = I_\nu^{-\infty}e - \sum_{i=1}^{N}\tau_i + \sum_{i=1}^{N} S_\nu^i(1-e^{-\tau_i})e - \sum_{j=1}^{i-1}\tau_j \tag{61}$$

where N is the number of frequency surfaces the beam has traversed and the subscripts and superscripts i and j label the frequency surfaces counting backward along the beam path.

A useful expression derived with the assumption of CRD in frequency and angle for the comoving frame line source function at P is

$$S^0 = \frac{(1-\epsilon^0)\bar{J}^0_{\rm ext} + G^0}{\epsilon^0 + (1-\epsilon^0)\tilde{\beta}}, \tag{62}$$

where ϵ^0 is the fraction of photons absorbed by the line that are not directly reemitted, G^0 is the nonscattering line source function which accounts for new line photons due to collisional excitations and transitions from other levels and the continuum, $\tilde{\beta}$ is the Sobolev escape probability, and $\bar{J}^0_{\rm ext}$ is the mean integrated specific intensity. All the quantities used to evaluate S^0 are evaluated at P. The observer frame line source functions appearing in equations (60) and (61) are obtained by multiplying S^0 by $[\gamma(1-\mu\beta)]^{-3}$ (see eqs. [2] and [6]). The escape probability is given by

$$\tilde{\beta} = \oint \frac{1-e^{-\tau}}{\tau}\frac{dw_0}{4\pi}, \tag{63}$$

where the integration is over all solid angle. For homologous expansion in the classical case, $\tilde{\beta} = (1-e^{-\tau})/\tau$ since the classical homologous expansion Sobolev optical depth is direction-independent (see eq. [55]). (Note that we use $\tilde{\beta}$ as the Sobolev escape probability symbol in this paper rather than the conventional β [e.g., RH; HS] since we require β for its even more strongly conventional use as v/c.) The mean integrated specific intensity is given by

$$\bar{J}^0_{\rm ext} = \oint [\gamma(1-\mu\beta)]^3 I^{-\infty}_{\nu_P}\left(\frac{1-e^{-\tau}}{\tau}\right)\frac{dw_0}{4\pi}. \tag{64}$$

The equation (62) is exactly as in the classical Sobolev method, except that there is no distinction between comoving frame and observer frame quantities in the classical case. To evaluate S^0 requires doing the integral for $\bar{J}^0_{\rm ext}$ accounting for all other relevant lines using the CP frequency surfaces and any continuum-radiating surfaces that may be present such as a central continuum-radiating core. In a classical general expansion case (see, e.g., RH) and in any homologous expansion case (see § 3), $\bar{J}^0_{\rm ext}$ will not depend on the line for which it is being evaluated, but only on bluer lines. Thus, if ϵ^0, G^0, and all continuum sources of flux were known, equation (62) would allow an explicit evaluation of all line source functions by starting from the bluest line considered and evaluating each line source function for the whole atmosphere in order of decreasing frequency. In a classical general contraction case with the same knowns, the same procedure could be followed, except that one would start from the reddest line and proceed blueward. In cases with nonmonotonic velocity fields, a line source function will in general depend nonlocally on itself (i.e., there will be remote self-coupling of the line in general) and on the source functions of redder and bluer lines. RH consider the classical Sobolev method treatment of nonmonotonic velocity fields. In extremely relativistic atmospheres in general expansion, there is also a possibility of remote self-coupling and dependence of the line source functions on both redder and bluer lines. Such relativistic effects arise for exponentially expanding atmospheres as we show in the Appendix. At present, there is no observational need to invoke these relativistic effects and the techniques for evaluating line source functions when they occur have not been worked out.

For simple calculations, one can introduce reasonable prescriptions for ϵ^0 and G^0. For example, if a core continuum flux has a higher temperature than the atmospheric temperature above the core (which is the usual situation), then it is natural to assume that lines with lower levels that are ground levels or metastable levels have their source functions mostly determined by excitation from their lower levels by the core continuum flux. Thus, a reasonable approximation is to treat these lines as pure scattering lines by setting ϵ^0 and G^0 to zero. With this approximation, equation (62) reduces to

$$S^0 = \frac{\bar{J}^0_{\rm ext}}{\tilde{\beta}}. \tag{65}$$

Equation (65) is essentially the same as HS's equation (34) for the Sobolev line source function in the pure scattering case. The Sobolev optical depths of the lines can be determined using LTE occupation numbers or some simple prescription.

For more exact self-consistent radiative transfer calculations, the line source functions and opacities must in general be obtained from a non-LTE calculation of the atomic occupation numbers. A Sobolev method non-LTE calculation uses the $\bar{J}^0_{\rm ext}$ and $\tilde{\beta}$ values for all relevant lines in the determination of these atomic occupation numbers (Klein & Castor 1978).

If instead of assuming CRD in angle (in the comoving frame), one assumes that a hybrid phase matrix (a linear combination of the Rayleigh phase matrix and the isotropic scattering phase matrix) applies (in the comoving frame), then it is possible to develop a formalism for the determination of the relativistic Sobolev line source Stokes vector. The line source Stokes vector (which is analogous to the line source function) is the quantity needed to treat polarized radiative transfer for which nonisotropic scattering is of most interest. The formalism for the line source Stokes vector is analogous to the formalism leading to equation (62). Papers by Jeffery (1988, 1989, 1990) have shown how the hybrid phase matrix can be incorporated in the classical Sobolev method in order to treat polarized radiative transfer. The expressions developed in these papers for the line source Stokes vector will also hold for the relativistic Sobolev method provided they are regarded as relating comoving frame quantities. For spherically symmetric atmospheres, one can use the analytic expressions for the line source Stokes vector given by Jeffery (1990, eqs. [37a] and [37b]). For axisymmetric atmospheres (Jeffery 1989) and three-dimensional atmospheres (Jeffery 1990), there are matrix equations that must be solved to obtain the line source Stokes vector. These matrix equations can be solved by ordinary numerical means or cumbersome analytic expressions could be developed. The simple analytic expressions for the line source Stokes vector obtained for the classical spherically symmetric, axisymmetric, and three-dimensional homologous expansion cases cannot be made relativistic because these expressions demand direction-independent Sobolev line optical depths which are not available in the relativistic homologous expansion case (see eq. [54]). Note that the axisymmetric and three-dimensional atmospheres would have to possess spherically symmetric velocity fields in order for the relativistic Sobolev formalism developed in this section to apply.

No consideration has yet been given to the relativistic Sobolev method treatment without the assumption of CRD in frequency.

The procedures for evaluating the net flux from an atmosphere using the Sobolev method formal solution (i.e., eqs. [60] or [61]) and for evaluating the mean integrated specific intensity in the relativistic case are essentially the same as in the classical case. One must, however, account for all transformations of frequencies, specific intensities, angles, etc., between the different frames (see eqs. [2]–[7]). The net effect of these transformations (as was discovered in doing the calculations for the demonstration spectra presented in § 6) is at least as important for a relativistic Sobolev method calculation as the effects of the relativistic CD and CP frequency surfaces. We discuss the use of the CD and CP frequency surfaces briefly in §§ 2 and 3, respectively. Relevant discussions of the procedures of classical Sobolev method calculations are given by, e.g., Mihalas (1978, p. 471), RH, Bartunov & Mozgovoi (1987), and Jeffery & Branch (1990). HS provide a detailed discussion of several kinds of calculations with the relativistic Sobolev method.

Finally, it should be noted that the implementation of all the relativistic effects that constitute the relativistic Sobolev method in an existing Sobolev method computer code for homologously expanding atmospheres is straightforward.

5. STATIONARITY, ADVECTION, AND THE RELATIVISTIC SOBOLEV METHOD AS APPLIED TO SUPERNOVAE

In developing the relativistic Sobolev method for supernovae, we have not so far made the stationarity approximation: i.e., assumed that the radiative transfer in supernovae could be approximated as time-independent. Our formalism for the CD and CP frequency surfaces accounts for expansion of the atmosphere during the flight time of the photons (see §§ 2 and 3). Thus, if one knew all the atomic occupation numbers and continuum radiation sources as functions of time, one could calculate the time-dependent emergent flux with the formalism we have developed. However, most supernova calculations using the Sobolev method do not attempt a time-dependent treatment and use the stationarity approximation for the atomic occupation numbers and continuum radiation sources. Supernovae are, of course, primary examples of rapidly varying astrophysical objects, so some justification for the stationary approximation is needed. Since the Sobolev method is principally concerned with radiative transfer in the outer atmosphere above the photosphere (i.e., where the continuum is optically thin), it is interesting to address the issue for that region of supernovae. (In this paper, the term photosphere denotes that atmosphere layer which is at approximately a continuum optical depth of 2/3.)

Consider a supernova with a photospheric velocity $v_{\rm ph}$. The effective velocity width of the atmosphere above the photosphere is very roughly $\sim v_{\rm ph}$. Consider only pure scattering in lines and continuum, since this should give the main outer atmosphere behavior. Most photons emitted from the photosphere will interact with 0, 1, or 2 lines and with continuous opacity of order once before escaping the atmosphere. Note that each line interaction will, in general, consist of several scattering events in a resonance region. For the moment, consider only the flight time; we will justify the neglect of the interaction time in resonance regions below. The flight time $\Delta t_{\rm flight}$ will typically be of the order of $mv_{\rm ph}\,t/c$, where m is roughly the number of line and continuum interactions an atmosphere-escaping photon undergoes and is a factor of order a few at most, and t is time since the explosion. Thus, the ratio of flight time to time since explosion is given approximately by

$$\frac{\Delta t_{\rm flight}}{t} \approx \frac{mv_{\rm ph}}{c} . \tag{66}$$

Since t is the evolutionary time scale of a supernova, the smaller $\Delta t_{\rm flight}/t$ is, the better the stationary approximation. One might guess that stationarity would be a rather good approximation for $\Delta t_{\rm flight}/t \approx 0.1$ and would become only marginally good for $\Delta t_{\rm flight}/t \approx 0.5$. The range of known supernova photospheric velocities is very roughly 1500–15,000 km s^{-1}; most observed photospheric velocities, however, fall in the range $\sim$5000–12,000 km s^{-1}. The photospheric velocity is not, of course, fixed for a given supernova, but decreases in time as the ejecta decreases in density and the photosphere recedes into the ejecta. The photospheric velocity evolution of Type II supernova SN 1987A exhibited the entire $\sim$1500–15,000 km s^{-1} range if day 100 of that event is taken as the end of its true photospheric epoch (Jeffery & Branch 1990, Fig. 16). The only other supernovae (of which the author is aware) for which photospheric velocities as high as of order 15,000 km s^{-1} have been determined are Type Ia supernovae SN 1984A (Branch 1987) and SN 1990N (JLK). Since typically $m \lesssim 3$, we conclude that $\Delta t_{\rm flight}/t \lesssim 0.15$ in the most cases. Thus, the stationary approximation is reasonably well justified for radiative transfer in supernovae above the photosphere even for the highest observed supernova photospheric velocities.

A second concern for the application of both the relativistic or classical Sobolev methods to supernovae is the neglect of advection, the outward transport of energy by the flow of matter. Considering only pure scattering in lines and neglecting all relativistic effects since only an approximate result for supernova-like velocities is of interest, the mean time that a photon is trapped in a resonance region and thus being advected is given approximately by

$$\Delta\bar{t}_{\rm ad} \approx \bar{n}\left(\frac{v_{\rm th}\,t}{c} + \Delta t^0_{\rm ex}\right) , \tag{67}$$

where $\bar{n}$ is the mean number of scattering events, t is again the time since explosion, $v_{\rm th}\,t$ is resonance region width for homologous expansion in the classical limit assuming the Lorentzian wings, of the line profile and microturbulence are negligible (see eqs. [56], [58], and [59]), $v_{\rm th}\,t/c$ is the characteristic flight time between scattering events in the resonance region, and $\Delta t^0_{\rm ex}$ is the comoving frame mean duration of a line excitation. For typical supernova temperatures of order 10^4 K (implying $v_{\rm th}$ of order $\sim$1–10 km s^{-1}) and for observable epochs (which typically begin $\sim$10 days after explosion and very rarely $\sim$1 day after explosion and last till of order hundreds of days), one finds that $v_{\rm th}\,t/c$ is unlikely to be smaller than $\sim$0.3 s. For important lines, $\Delta t^0_{\rm ex}$ will be 10^{-8} s to within about 3 orders of magnitude. Thus, it is clear that the second term in equation (67) is negligible. The Sobolev expression for $\bar{n}$ in the classical homologous expansion case is

$$\bar{n} = \tau \tag{68}$$

(e.g., Jeffery 1991b). Therefore, neglecting the second term and substituting for $\bar{n}$, equation (67) becomes

$$\Delta\bar{t}_{\rm ad} \approx \frac{\tau v_{\rm th}\,t}{c} . \tag{69}$$

The importance of advection clearly increases with the ratio of advection length l_{ad} to the characteristic size of the supernova l_{char}. This ratio is approximately given by

$$\frac{l_{ad}}{l_{char}} \approx \frac{v_{ph}\Delta\bar{t}_{ad}}{v_{ph}t} \approx \frac{\tau v_{th}}{c} . \quad (70)$$

For typical values of v_{th}, equation (70) predicts that advection will become very important for $\tau \gtrsim 3 \times 10^4$. With optical depths of this size, assumption of negligible Lorentzian wings will usually be rather poor (e.g., Hummer & Rybicki 1992). Above the photosphere, however, lines with optical depths that are at all near this 3×10^4 (at least above 2000 Å) seem to be very rare. Lines that form strong profiles in supernova spectra typically have optical depths of order 100 or less above the photosphere. Therefore, typically $l_{ad}/l_{char} \lesssim 0.003$ and the neglect of advection for line transfer above the photosphere is very well justified. It has been shown, however, that advection is quite important for radiative transfer below the photosphere (Hauschildt et al. 1991). This is clearly because of the strong photon trapping in optically thick expanding layers. Thus, Sobolev method calculations of deep radiative transfer can only be of qualitative accuracy.

To validate the neglect of the line interaction time in the discussion of stationary approximation, consider the ratio

$$\frac{m\Delta\bar{t}_{ad}}{\Delta t_{flight}} \approx \frac{\tau v_{th}}{v_{ph}} . \quad (71)$$

For typical values of v_{th} and v_{ph}, this ratio will be small when $\tau \ll 10^3$. Since $\tau \gtrsim 10^3$ rarely occurs above the photosphere, the neglect of the line interaction time in the discussion of the stationarity approximation is justified.

The conclusion of this section is that the use of the stationarity approximation and the neglect of advection are justified in Sobolev method line radiative transfer calculations for supernova atmospheres above the photosphere.

6. DEMONSTRATION SPECTRA

In this section, some demonstration spectra calculated using the relativistic and classical Sobolev methods for models in homologous expansion are presented and compared. Demonstration relativistic spectra calculated using velocity fields considered appropriate for stellar wind atmospheres are reported by HS. For the relativistic calculations, we made the stationarity approximation for the atomic conditions and chose the characteristic time for the models to the observer time (see the discussion in § 2). For the classical calculations, the stationarity approximation has been made for both the atomic conditions and the photon flow, and the characteristic time was again chosen to be the observer time. The stationarity approximation for photon flow means, of course that observer-directed beams have constant β_p (see § 2). In order to conform to most usual format, the spectra are given in the f_λ representation rather than in the f_ν representation and are plotted versus wavelength rather than frequency. Note that

$$I_\nu = I_\lambda \frac{\lambda^2}{c} , \quad I^0_{\lambda_0}\lambda_0^5 = I_\lambda \lambda^5 . \quad (72)$$

An important detail of the classical calculations is that equations (15) and (50) were used to calculate the CD and CP frequency surfaces, respectively. Alternative expressions for the classical CD and CP frequency surfaces are $\beta_z^{1st} = 1 - \nu_0/\nu$ and $\Delta\beta^{1st} = 1 - \nu_1^0/\nu_2^0$. The two sets of classical CD/CP frequency expressions are equally valid and give identical sets of results when second-order terms are actually negligible. When second-order terms are not negligible, however, the two sets of expressions will yield different sets of results which will, of course, both be in error to some degree. Because of the high velocities used for the calculation of classical spectra presented here, these classical spectra are only exactly reproducible using equations (15) and (50).

The model (which will be called the schematic model) used for first three comparison calculations consists of a core which radiates a wavelength-independent angle-independent continuum flux surrounded by a line scattering atmosphere: no continuous opacity is included. The core and atmosphere are both in homologous expansion. The core velocity and the core Sobolev optical depths are parameters. Above the core, a line optical depth is made to scale as an inverse exponential of velocity: thus

$$\tau = \tau_{core}\, e^{-(v - v_{core})/v_e} , \quad (73)$$

where v_{core} is the core velocity, τ_{core} is the core optical and the parameter v_e is the e-folding velocity of the atmosphere. Artificial lines with pure scattering line source functions were used.

Figure 4 shows the first comparison between relativistic and classical spectra. The spectra have been normalized to their continuum flux levels. The core velocity and e-folding velocity for the calculation were 15,000 km s^{-1} and 2500 km s^{-1}, respectively. These atmospheric velocities are roughly those of Type Ia SN 1990N at its earliest observed epoch; SN 1990N is one of the supernovae with the highest observed photospheric and ejecta velocities (see §§ 1 and 5 and JLK). The outer boundary velocity of the atmosphere was set effectively to infinity. Only a single line of line center wavelength 3000 Å was included in the calculations. The core Sobolev optical depth of the line was 10^3 and thus the line was strong; the Ca II H and K lines in SN 1990N were of comparable strength in the earliest observed epoch and gave rise to that supernova's broadest observed P Cygni line. Both the relativistic and classical line profiles seen in Figure 4 are typical P Cygni profiles with emission features centered near the line center wavelength and blueshifted absorptions. The slope change near ~2850 Å in both profiles is due to the fact that the CD frequency surfaces for wavelengths above ~2850 Å intersect the core while those for wavelengths below ~2850 Å do not. The blue edge of the relativistic absorption shows that ejecta moving as fast as ~40,000 km s^{-1} is important for line formation.

The normalization of the spectra in Figure 4 hides the fact that they have different overall energy scales. The ratio of the relativistic continuum flux to the classical continuum flux is in fact 1.2. This extra energy in the relativistic case is due to the correct relativistic treatment of energy exchanges between radiation and the matter's (macroscopic) kinetic energy. The energy exchange is mainly a consequence of the $(\lambda_0/\lambda)^5$ transformation factor in the Lorentz transformation of specific intensity (see eq. [72]). For an emitting moving source, this factor gives rise to an enhancement of blueshifted (i.e., forward) emission and reduction of redshifted (i.e., backward) emission; the effect is sometimes called the relativistic beaming effect. Since the core hemisphere facing the observer is moving toward the observer, $\lambda < \lambda_0$, and thus there is a continuum flux enhancement in the observer frame. For matter moving toward the observer at the core velocity $(\lambda_0/\lambda)^5 = 1.28$; since most of the core has a smaller velocity in the observer's direction than

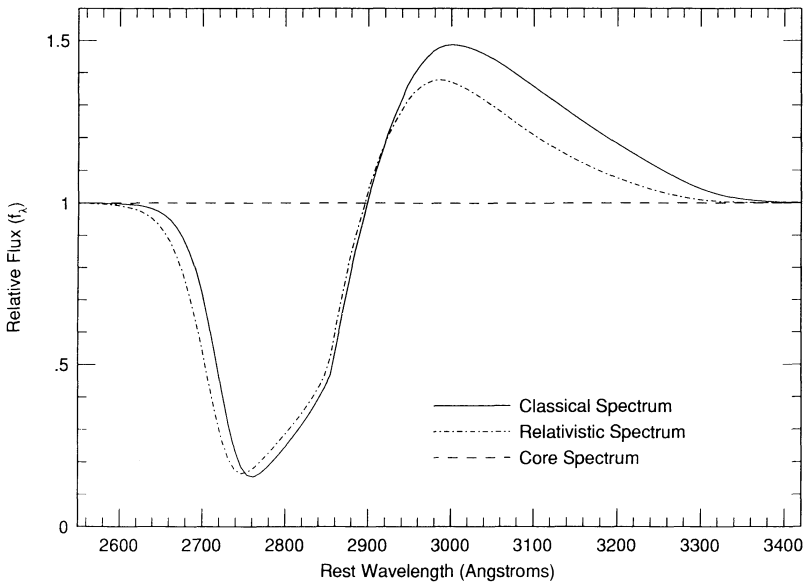

FIG. 4.—Relativistic and classical spectra calculated for the homologously expanding schematic model. The core velocity is 15,000 km s^{-1}. Only one line with a line center wavelength of 3000 Å is included in the schematic model atmosphere.

15,000 km s^{-1}, the continuum flux enhancement we calculated is less than 1.28. The extra continuum flux energy must be thought of as coming at the expense of the matter's kinetic energy. Since the $(\lambda_0/\lambda)^5$ transformation factors are not employed in the classical calculation, no such continuum flux enhancement occurs for the classical spectrum.

It should be noted that the treatment here assumes that the matter's kinetic energy is too large to be perturbed by energy exchanges with the radiation field. This assumption is well justified for supernovae which have total kinetic energies of order 10^{51} ergs and luminosities near-maximum light of order 10^{43} ergs s^{-1} for Type Ia's and $\gtrsim 10^{42}$ ergs s^{-1} for other types. Supernovae do not stay at maximum light very long and decline in luminosity by an order of magnitude or more over a period of tens of days. Thus, it is clear that even over 100 days the total radiation energy processed by a supernova atmosphere will be much less than the supernova's total kinetic energy; the total energy exchange between the total radiation energy and the supernova's total kinetic energy will be smaller still. It follows that over shorter time periods, the energy exchanges will be negligible for the matter's kinetic energy.

It is the Lorentz transformation of specific intensity that is primarily responsible for the differences between the emission features in the relativistic and classical spectra. In both relativistic and classical cases, the emission feature flux comes from the atmosphere limb and was originally mostly blueward of the line center wavelength in the observer frame and directed roughly perpendicularly to the line of sight. After being redirected toward the observer by scattering through large angles, the emission feature flux is more centered about the line center wavelength. The $(\lambda_0/\lambda)^5$ transformation factors ensure that in the relativistic case energy is lost in the emission feature formation; this energy loss does not happen in the classical case. The loss of emission feature flux energy in the relativistic case results in the smaller emission feature relative to the continuum flux level. The transformation factors also enhance the blue side and reduce the red side of the relativistic emission feature. This effect is partially responsible for the blueshift of the relativistic spectrum's maximum by 15 Å from 3000 Å (i.e., by 0.5% of the line center wavelength). The relativistic CD frequency surfaces are the other partial cause of this blueshift. In the classical spectrum, the maximum is right at the line center wavelength as one would expect.

The differences between the absorptions in the two spectra are mostly due to the difference between the relativistic and classical CD frequency surfaces. One notable difference is that the blue side of the relativistic absorption is $\sim$10–20 Å blueward of the blue side of the classical absorption. Both blue sides, of course, form in about the same location in the model atmosphere. If we tried to fit the relativistic absorption blue side with the classical one, we would have to make the layers of blue side formation $\sim$1000–2000 km s^{-1} faster in the classical calculation. Clearly, a classical fitting procedure would be somewhat in error for observed supernova P Cygni absorptions as broad as those shown in Figure 4.

The difference in optical depth treatment between the relativistic and classical Sobolev method gives rise to differences in the spectra which are noticeable, but less important than those due to the Lorentz transformation of specific intensity and the different CD frequency surfaces. The differences in the spectra due to the different treatment of the angles are very small because of the first-order agreement in the relativistic case between μ_{1*} and μ_1^0 (see § 3) results in a nearly classical photon-flow-stationary treatment of angles; at higher ejecta velocities significant spectral differences do arise because of the different treatment of angles.

The moderate profile differences and the overall energy scale difference between the spectra shown in Figure 4 show that relativistic effects are not negligible for atmospheres with velocity fields as fast as those in the fastest observed supernovae.

Figure 5 shows relativistic and classical spectra calculated with exactly the same parameters as for the Figure 4 spectra, except that a second artificial line with line center wavelength 3300 Å and core optical depth 10^3 has been included in the calculations. Thus, once again, the ratio of relativistic contin-

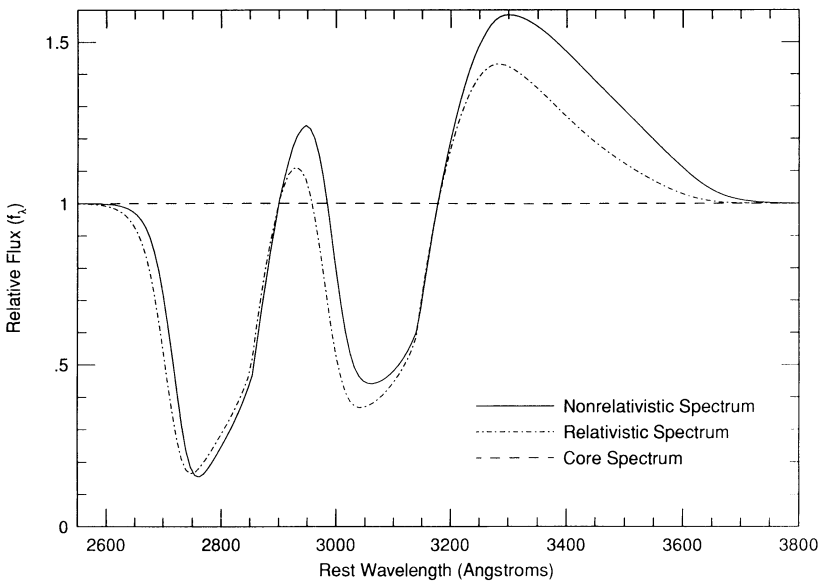

FIG. 5.—Relativistic and classical spectra calculated for the homologously expanding schematic model. The core velocity is 15,000 km s^{-1}. Two lines with line center wavelengths of 3000 and 3300 Å are included in the schematic model atmosphere.

uum flux to classical continuum flux is 1.2. Both spectra show typical examples of blended P Cygni profiles. The absorptions of the 3300 Å line largely suppress the emission features of the 3000 Å line. This suppression is consistent with past experience which shows that P Cygni absorption generally tend to dominate overlapping emission features. Because of this general behavior, it is often much easier to identify absorptions than to identify emission features in observed spectra; consequently, the absorptions are usually the features that are labeled in figures. If the two artificial lines were moved farther and farther apart, the profiles would approach the appearance of and eventually become noninteracting P Cygni line profiles. If the two model lines were moved closer and closer together and finally made coincident, the profiles would converge to a single line profile. Demonstration spectra (calculated with the classical Sobolev method) showing the behavior as two lines are moved from wide separation to the same wavelength are given by Jeffery & Branch (1990, Figs. 10–11). For the case of pure scattering lines, a single line profile due to two coincident lines of equal strength would be identical to the line profile of one of the lines acting alone if its optical depths were doubled everywhere (e.g., Jeffery & Branch 1990, p. 193). One should note that the size of the line features for strong lines (i.e., those with Sobolev optical depths greater than of order 1 over a substantial part of the atmosphere) tend to vary much more weakly than linearly with optical depth (e.g., Jeffery & Branch 1990, pp. 188–189); thus, doubling the optical depths of a strong line will cause a much smaller than twofold change in the size of line profile features.

A calculation has been done that was identical to the one yielding the relativistic spectrum in Figure 5, except that classical CP frequency surfaces were used. The redder profile (i.e., the line features redward of $\sim$2950 Å) of the resulting semi-relativistic spectrum differed from the redder profile of the fully relativistic spectrum by being lower by less than $\sim$1% of the continuum flux level; the differences between the profiles were most noticeable at the bottoms of the absorptions and at the tops of the emission features. The bluer profiles (i.e., the line features blueward of $\sim$2950 Å) of the semi relativistic and fully relativistic spectra were identical. This is to be expected since in homologously expanding atmospheres a bluer line cannot interact with photons coming from a redder line (see §§ 3 and 4). Once can see that the difference between the use of relativistic and classical CP frequency surfaces is very small for velocity fields of the scale we are using.

Figure 6 presents relativistic and classical spectra calculated with parameters that make the schematic model much more relativistic than in the calculations for Figures 4 and 5. The core and e-folding velocities were set to 2.0×10^5 km s^{-1} [i.e., to $\sim(2/3)c$] and 20,000 km s^{-1}, respectively. The outer boundary of the atmosphere was set to a velocity of 2.7×10^5 km s^{-1} (i.e., to $0.9006c$). The velocity width of the atmosphere is only 35% of the core velocity, and thus the atmosphere is geometrically thin. Only a single artificial line of line center wavelength 3000 Å and core Sobolev optical depth 10^3 was included in the calculations. The Sobolev optical depth of this line falls to only 30 at the outer boundary. Thus, the line is in fact saturated throughout the atmosphere: i.e., $e^{-\tau} \ll 1$ everywhere in the atmosphere. This means that nearly all of the flux emergent from a resonance region will be due to the source function, not to the incident beam (see eq. [60]).

For the choice of parameters we have made, the schematic model is unlike any known physical system. It is implausible, as can be seen from equation (66), that the stationarity approximation for atomic conditions would be valid for a system with the velocity field we have set up. The use of a wavelength-independent core continuum flux is unrealistic for wavelength intervals as large as are needed to calculate the broad profiles in Figure 6. We have continued to use the wavelength-independent core continuum flux, however, because it is the neutral choice. Because the schematic model in this case is so unrealistic, the spectra we have calculated using it are intended only to demonstrate extreme relativistic effects.

The classical line profile is exactly what one would expect for a model with the parameters described; it is remarkable only because of its very large wavelength width. The explanation of

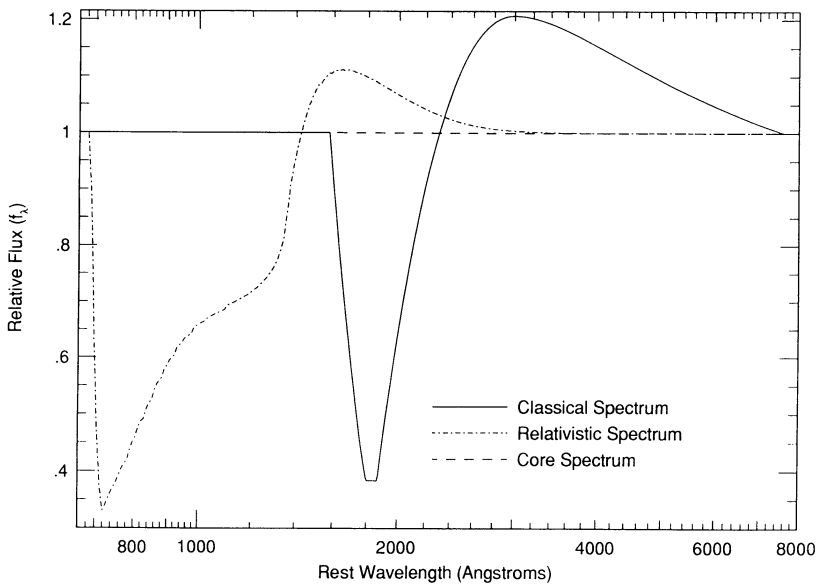

FIG. 6.—Relativistic and classical spectra calculated for the homologously expanding schematic model. The core velocity is 2.0×10^5 km s^{-1} [i.e., $\sim(2/3)c$], and thus the model is much more relativistic than in the cases for Figs. 4 and 5. Only one line with a line center wavelength of 3000 Å is included in the schematic model atmosphere.

the special features of this profile is as follows. The blue side of the absorption is caused by the classical CD frequency surfaces (which, we recall, are planes perpendicular to the line of sight) that are on the near side of the ejecta and do not intersect the core. As a CD frequency surface is moved farther away from the core (i.e., as it becomes a CD frequency surface for smaller wavelength), there is an increasing annulus about the line of sight where beams from the core never intersect the (physical) CD frequency surface. This annulus grows until it is the entire projected area of the core; when this happens the flux has returned to the continuum level. The blue edge of the absorption shows a slope discontinuity because the Sobolev line optical depth is large out to the outer boundary and then goes to zero discontinuously. The flat bottom of the absorption is also due to the thin shell geometry of the atmosphere which causes the emergent flux for the wavelength range corresponding to the line of sight velocities between $(v_{\rm outer}^2 - v_{\rm core}^2)^{1/2}$ and $v_{\rm core}$ (where $v_{\rm outer}$ is the outer boundary velocity) to be wavelength-independent when the core flux is wavelength-independent (e.g., Jeffery & Branch 1990, p. 192). The classical emission feature is limited in wavelength because the line-of-sight extent of the atmosphere limb is only from $(v_{\rm outer}^2 - v_{\rm core}^2)^{1/2}$ to $-(v_{\rm outer}^2 - v_{\rm core}^2)^{1/2}$. The classical planar CD frequency surfaces with line-of-sight velocities more negative than $-(v_{\rm outer}^2 - v_{\rm core}^2)^{1/2}$ have no surface area inside the atmosphere that is not occulted by the core, and so only the core flux emerges at the redshifted wavelengths corresponding to these CD frequency surfaces. The sharp cutoff of limb emission due to occultation causes the discontinuity in spectrum slope at the red edge of the emission feature at 7600 Å.

The relativistic P Cygni profile in Figure 6 is much more blueshifted than the classical P Cygni profile and has a rather different shape. As for the calculations for Figures 4 and 5, the greater blueshift of the absorption is mainly due to the relativistic CD frequency surfaces and the blueshift of the emission feature is mainly due to the combined effect of the Lorentz transformation of the specific intensity and relativistic CD frequency surfaces. The other changes in shape from the classical spectrum are not, however, easily understood; all relativistic effects play a role in causing them. The steep rising blue side of the absorption and the discontinuity in slope at the blue edge of the absorption are the same as in the classical case and have essentially the same explanation. One distinction, however, is that because the beam paths in the comoving frame do not constant β_p values, but have β_p values that coverage to zero as β_z goes to 1 (see Fig. 1), the annuli where beams from the core can evade the CD frequency surfaces occur only for CD frequency surfaces whose z-axis velocities are $\gtrsim 0.89c$; i.e., whose z-axis velocities are much higher than $v_{\rm core}$. Since the atmosphere ends at $0.9006c$, the blue side of the relativistic absorption is steeper than in the classical case.

Just as with the relativistic and classical spectra in Figures 4 and 5, the overall energy scale of the relativistic and classical spectra in Figure 6 is different. Because of the much higher velocities used for the Figure 6 spectra, there is a much greater enhancement of the relativistic spectrum's energy relative to the classical spectrum's energy than for the spectra of Figures 4 and 5. The ratio of relativistic continuum flux to classical continuum flux for the Figure 6 spectra is 55. For matter moving toward the observer at the core velocity $(\lambda_0/\lambda)^5 = 56$ which is very close to the calculated enhancement factor for the continuum flux.

The relativistic and classical spectra for the final comparison were calculated using a realistic supernova model. This model is essentially the same model that JLK used for an analysis of the photospheric epoch spectra of Type Ia supernova SN 1990N. The model has a total mass of 1.4 $M_\odot$, and thus conforms to the standard picture of Type Ia's in which the Type Ia progenitors are white dwarfs with masses near the Chandrasekhar mass. The model is in homologous expansion and has an inverse exponential density profile with e-folding velocity 3160 km s^{-1}. The composition of the model is displayed in JLK's Figure 1. This composition is a modified version of the composition of the deflagration model W7 of Nomoto, Thielemann, & Yokoi (1984) and Thielemann, Nomoto, & Yokoi (1986). For our calculation, the spectrum is mostly formed

above $\sim 15{,}000$ km s^{-1} where the composition does not come from model W7, but instead was constructed by JLK in order to fit the early spectra of SN 1990N. This outer composition is homogeneous and the dominant elements in descending order by mass fraction are oxygen (0.53), carbon (0.36), magnesium (0.034), silicon (0.032), sulfur (0.018), neon (0.0092), argon (0.0038), and calcium (0.0032). The iron peak elements have smaller abundances, but due to their large line opacities they are very significant for spectrum formation. The iron peak elements are not in solar ratio and are dominated by radioactive ^{56}Ni, not iron, at the explosion epoch. The radioative ^{56}Ni gives rise to the decay chain $^{56}\text{Ni} \rightarrow {}^{56}\text{Co} \rightarrow {}^{56}\text{Fe}$, where the half-lives of ^{56}Ni and ^{56}Co are 6.10 and 77.12 days, respectively (Huo et al. 1987).

The earliest observed SN 1990N spectrum (which is the earliest observed spectrum for any Type Ia) is from 1990 June 26, 14 days before maximum light (i.e., before the B maximum). This spectrum comes from at least 3 days after the explosion (Leibundgut et al. 1991). Following JLK, we assume that the epoch of the spectrum is 6 days after maximum and chose the density and ^{56}Ni:^{56}Co:^{56}Fe ratio our model to simulate SN 1990N at that time. The core velocity density, and temperature of the model were set to 13,000 km s^{-1}, 3.38×10^{-13} g cm^{-3}, and 14,000 K, respectively. The mass above the core is 0.274 $M_\odot$. At the electron photosphere (i.e., at an electron scattering opacity optical depth of 2/3) the velocity, density, and temperature of the model were 16,400 km s^{-1}, 1.43×10^{-13} g cm^{-3}, and 10,600 K, respectively. The temperature profile prescription of JLK has been assumed with $v_1 = 16{,}000$ km s^{-1} and $T_1 = 11{,}000$ K (see JLK for definitions of v_1 and T_1). The outer boundary of the model was set effectively to infinity. The Sobolev line optical depths were calculated for the model using LTE. The lines were all given Planck function source functions evaluated at the local temperature (i.e., ϵ^0 was set to 1 and G^0 to $\epsilon^0 B^0_\lambda$ in the source function; see eq. [62]). All lines included in Kurucz's line data files (Kurucz 1991) belonging to the relevant ions were used in the calculations; thus, the quasi-continuous expansion opacity due to overlapping lines arose naturally in the calculations. The only other continuous opacity included is electron scattering opacity which is treated using the discretized continuous opacity approximation (Jeffery 1989, 1991b; JLK).

The June 26 SN 1990N spectrum is shown in Figure 7 along with the relativistic and classical spectra calculated using our model. The scale of the relativistic spectrum is set by forcing it to have the same integrated flux as the observed spectrum in the wavelength range 4300–5900 Å. The scales of the relativistic and classical spectra are in their calculated ratio. The ratio of the relativistic and classical core fluxes varies over the narrow range 1.1645–1.1709; the variation is due the slow variation of the core flux with wavelength. The cause for the difference in core fluxes is the same as described for the core spectra in Figures 4, 5, and 6. The emergent synthetic spectra have a variable ratio with a mean of 1.13; we expected this ratio to vary based on the earlier demonstration results. Figure 7 shows that the relativistic spectrum is very similar in shape to the classical spectrum. As we could expect from the earlier demonstration results, the relativistic line profiles are blue-shifted relative to the classical line profiles. The distinction between the relativistic and classical spectra is small. If we had fitted the scale of the classical spectrum to that of the observed as we did for the scale of the relativistic spectrum, then the distinction would be even smaller. Since distinction between the observed and relativistic spectra is much larger than that between the relativistic and classical spectra, the lack of relativistic effects in the classical calculation is not the limiting error in the classical calculation. Nevertheless, it is clear that truly accurate calculations would need to be relativistic especially if one did attempt to calculate the absolute flux scale.

Although we are not concerned with analyzing the SN 1990N spectrum, a few remarks can be made. A full analysis of the SN 1990N spectrum is given by JLK. The SN 1990N spectrum is a combination of *IUE* UV and CTIO optical spectra; the spectra are joined at ~ 3200 Å. The absolute scale of the

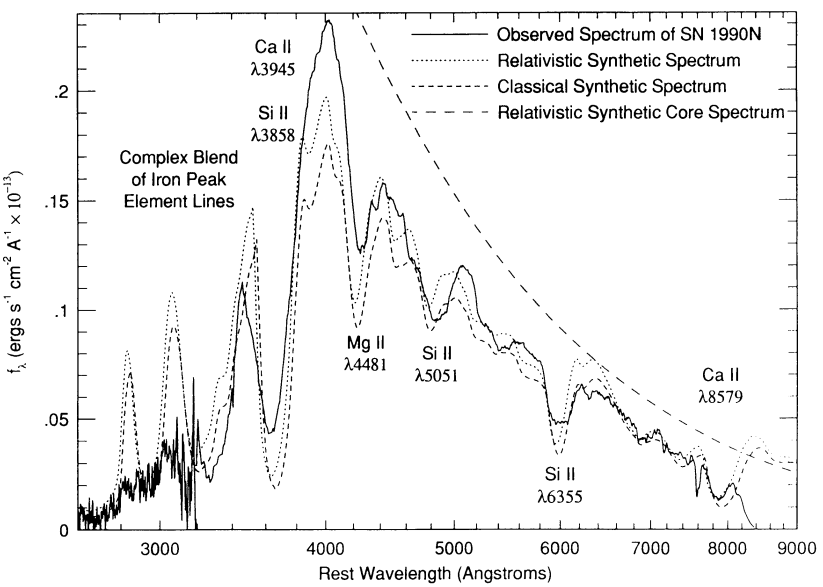

FIG. 7.—Relativistic and classical synthetic spectra calculated for a realistic Type Ia model and the observed 1990 June 26 spectrum of SN 1990N. The model parameters were chosen in order to fit the SN 1990N spectrum which comes from 14 days before maximum light and is the earliest Type Ia spectrum observed.

IUE spectrum is accurate to ~10%. The optical spectrum required a correction factor based on photometry in order to set the absolute scale. Unfortunately, the V photometric correction factor was 1.600 and the B photometric correction factor was 1.259 (Schmidt 1992). The V photometric correction factor was deemed to be somewhat more reliable and was adopted here. The redward of ~8070 Å, the SN 1990N spectrum is decreasing with wavelength. This decreasing region is physically unlikely, and there are reasons to believe the spectrum may be inaccurate at some point beyond ~7500 Å (Foltz 1992). Therefore, the discrepancy between the observed and synthetic spectra redward of ~8070 Å is not worrisome.

The synthetic spectra are lower than the synthetic core spectra (only the relativistic synthetic core spectrum is shown). In the optical this flux reduction is due mainly to backscattering to the core by electron scattering opacity and the much larger flux reduction in the UV is due mainly to line blanketing caused principally by iron peak element lines. The UV flux reduction is necessary to reproduce the well-known UV flux deficiency of Type Ia supernovae relative to blackbody fits to the optical. Our synthetic spectrum calculations reproduce the SN 1990N UV deficiency, but not all the details of the observed UV region. We have labeled some of the observed P Cygni absorptions with the multiplet designations. The identifications (made on the basis of synthetic spectrum fits) are the most certain ones that can be made; less certain identifications are discussed by JLK. The Si II λ3858 multiplet is of similar strength to the Si II λ6355 multiplet, but it is only a minor contributor to the large absorption centered at ~3650 Å; the Ca II λ3945 multiplet is the dominating contributor to this absorption.

7. CONCLUSIONS

We have derived the CD and CP frequency surface expressions and presented the other expressions needed for the implementation of the relativistic Sobolev method for the case of atmospheres in homologous expansion. This implementation in existing Sobolev method codes for homologously expanding atmospheres is straightforward. The prime astrophysical examples of homologously expanding atmospheres are supernovae. For the analysis of supernova atmospheres with the highest velocities observed, the relativistic Sobolev method treatment yields a small, but significant, improvement over the classical Sobolev method treatment. It is possible that supernovae with photospheric velocities and ejecta velocities much higher than 15,000 km s^{-1} and 40,000 km s^{-1}, respectively, will be observed in the future. For such cases, Sobolev method calculations would have to be relativistic. The relativistic Sobolev method offers a formal improvement over the classical Sobolev method in all cases.

I thank the referee, Phil Pinto, Bruno Leibundgut, and Bob Kirshner for their comments on this paper and Brian Schmidt for calculating the photometric correction factors for the SN 1990N spectrum. The research for the paper has been supported by NSF grant AST-89-05529 and NASA grant NAGW-1789.

APPENDIX

THE RELATIVISTIC SOBOLEV METHOD APPLIED TO EXPONENTIALLY EXPANDING ATMOSPHERES

Consider a spherically symmetric atmosphere with a velocity field given by

$$\beta = kr\,, \tag{A1}$$

where we again measure velocity in units of c and where k is a constant. This atmosphere is like a homologously expanding atmosphere in that velocity is proportional to distance, but unlike in that it is stationary and that matter elements instead of being in uniform motion are accelerating. As a function of time, the velocity of a matter element obeys

$$\beta = \beta_0\, e^{kt}\,, \tag{A2}$$

where β_0 is the matter element's initial velocity at t is the time since it started its motion. We will call this sort of velocity field exponential expansion. There is no astrophysical case of exponential expansion that we are aware of. However, a brief discussion of the application of the relativistic Sobolev method to the case of exponential expansion satisfies a formalism interest.

A little thought shows that the CD frequency surfaces for exponential expansion are the same as those for homologous expansion (see § 2 and Fig. 1). The distinction is that in exponential expansion the observer-directed beams follow paths of constant β_p. As one can see from Figure 1, there is a possibility of a beam interacting twice with the CD frequency surfaces for a single d value: i.e., of remote self-coupling in very relativistic atmospheres when the upper case relativistic CD frequency surfaces can become physical. As we showed in § 2, there must be matter with $\beta > (3)^{1/2}/2$ in order for this to occur. It is easily shown that the remote self-coupling is one way: i.e., a beam can interact with lower case CD frequency surface and then the upper case CD frequency surface, but a collinear beam going the opposite direction cannot interact with the two CD frequency surfaces in the reverse order. In this respect, the exponential expansion remote self-coupling is unlike the two-way remote self-coupling that can occur in nonrelativistic atmospheres with nonmonotonic velocity fields (see § 2 and RH). The possibility of remote self-coupling in exponential expansion cases was pointed out by HS, who do not, however, use the expression exponential expansion.

The general expression for the CP frequency surfaces (i.e., the general expression for $\Delta\beta$) for exponential expansion is quite different than that for homologous expansion. Using the same definitions as in § 3, this expression for a common point P_1 is

$$\Delta\beta = \Delta\beta_{\mp} = \mu_1\beta_1 - 1 + G \mp \sqrt{G^2 - G\beta_1^2(1-\mu_1^2)}\,, \tag{A3}$$

where

$$G = \frac{d_{12}^2\,\gamma_1^2(1-\mu_1\beta_1)^2}{1 + d_{12}^2\,\gamma_1^2(1-\mu_1\beta_1)^2}\,. \tag{A4}$$

For some parameter values one finds $\Delta\beta < 0$. In these cases, photons emitted from P_1 will interact with the line at a remote point a velocity interval $|\Delta\beta|$ away. There is no CP frequency surface where this occurs.

Because exponential expanding atmospheres are stationary, the beam path geometry in the observer and comoving frames is the same (see Fig. 2). Therefore, the expression for β_2 follows simply from the Law of Cosines:

$$\beta_2 = \sqrt{\beta_1^2 + \Delta\beta^2 - 2\Delta\beta(\mu_1\beta_1)} \,. \tag{A5}$$

The expression for μ_2 follows from equations (37) and (38)

$$\mu_2 = \frac{1 - d_{12}(\gamma_1/\gamma_2)(1 - \mu_1\beta_1)}{\beta_2} \,. \tag{A6}$$

The lower case solution for $\Delta\beta$ is the classical analog solution. This solution to second and first order in small δ_{12} and β_1 becomes

$$\Delta\beta_+^{2d} = \delta_{12}(1 - \tfrac{1}{2}\delta_{12}) \,, \tag{A7}$$

$$\Delta\beta_+^{1st} = \delta_{12} \,, \tag{A8}$$

respectively. The solutions both give spheres centered on the common point; the first-order solution is the classical solution itself. The second- and first-order classical analog solutions are identical to those obtained for the homologous expansion case (see § 3). No remote self-coupling is allowed to second order.

The general solutions for $\Delta\beta$ are physically meaningful (i.e., describe physical CP frequency surfaces) only when the discriminant of equation (A3) is greater than or equal to zero and, as explained above, when $\Delta\beta \geq 0$. Few simple ways of understanding the general behavior of the equation (A3) have been found. A full discussion of this general behavior is beyond the scope of this paper; here we will make only a few remarks. For $\delta_{12} < 0$ (a case for which no classical or second-order classical analog solution exists), both the upper and lower case solutions of equation (A3) can become physically meaningful, but only for β_1 very close to 1. For $\delta_{12} = 0$, the general solution reduces to

$$\Delta\beta = \begin{cases} 2[G - (1 - \mu_1\beta_1)] \,; \\ 0 \,. \end{cases} \tag{A9}$$

The zero solution of equation (A9) is just the local self-coupling solution. The upper case solution of equation (A9) gives the remote self-coupling solution. This solution is only physically meaningful when $\Delta\beta \geq 0$; it is easy to show that $\Delta\beta$ can become greater than 0 only when $\beta_1 > (3)^{1/2}/2$. Thus, as we already knew from a consideration of the CD frequency surfaces remote self-coupling can only occur for $\beta_1 > (3)^{1/2}/2$. For $\delta_{12} > 0$, the upper case solution of equation (A3) was never found to be physically meaningful in a numerical study of its behavior.

REFERENCES

Bartunov, O. S., & Mozgovoi, A. L. 1987, Astrophysics, 26, 136
Branch, D. 1987, ApJ, 316, L81
Branch, D., Doggett, J. B., Nomoto, K., & Thielemann, F.-K. 1985, ApJ, 294, 619
Castor, J. I. 1970, MNRAS, 149, 111
Eastman, R. G., & Kirshner, R. P. 1989, ApJ, 347, 771
Eastman, R. G., & Pinto, P. A. 1993, ApJ, in press
Foltz, C. B. 1992, private communication
Hamann, W.-R. 1981, A&A, 93, 353
Harkness, R. P. 1991a, in Supernovae: Proc. 10th Santa Cruz Workshop in Astronomy and Astrophysics, ed. S. E. Woosley (New York: Springer), 454
———. 1991b, in Proc. ESO/EIPC Workshop: SN 1987A and Other Supernovae, ed. I. J. Danziger & K. Kjär (Garching: ESO), 447
Hauschildt, P. H., Best, M., & Wehrse, R. 1991, A&A, 247, L21
Hummer, D. G., & Rybicki, G. B. 1985, ApJ, 293, 258
———. 1992, ApJ, 387, 248
Huo, J., Hu, D., Zhou, C., Han, X., Hu, B., & Wu, Y. 1987, Nucl. Data Sheets, 51, 1
Hutsemékers, D., & Surdej, J. 1990, ApJ, 361, 367 (HS)
Jeffery, D. J. 1987, Nature, 329, 419
———. 1988, Ph.D. thesis, McMaster University
———. 1989, ApJS, 71, 951
———. 1990, ApJ, 352, 267
———. 1991a, in Proc. ESO/EIPC Workshop: SN 1987A and Other Supernovae, ed. I. J. Danziger & K. Kjär (Garching: ESO), 257
———. 1991b, ApJ, 375, 264
Jeffery, D. J., & Branch, D. 1990, in Jerusalem Winter School for Theoretical Physics, Vol. 6, Supernovae, ed. J. C. Wheeler, T. Piran, & Weinberg (Singapore: World Scientific), 149
Jeffery, D. J., Leibundgut, B., Kirshner, R. P., Benetti, S., Branch, D., & Sonneborn, G. 1992, ApJ, 397, 304 (JLK)
Kirshner, R. P., et al. 1993, ApJ, 415, 589
Kirshner, R. P., Sonneborn, G., Crenshaw, D. M., & Nassiopoulos, G. E. 1987, ApJ, 320, 602
Klein, R. J., & Castor, I. J. 1978, ApJ, 220, 902
Kurucz, R. L. 1991, in Stellar Atmospheres: Beyond Classical Models, ed. L. Crivellari, I. Hubeny, & D. G. Hummer (Dordrecht: Kluwer), 441
Leibundgut, B., Kirshner, R. P., Filippenko, A. V., Shields, J. C., Foltz, C. B., Phillips, M. M., & Sonneborn, G. 1991, ApJ, 371, L23
Lucy, L. B. 1971, ApJ, 163, 95
———. 1987, in ESO Workshop on the SN 1987A, ed. I. J. Danziger (Garching: ESO), 417
Mazzali, P. A. 1988, in ESO SP-281, Vol. 2, A Decade of UV Astronomy with the *IUE* Satellite, ed. N. Longdon & E. J. Rolfe (Noordwijk: ESA), 163
———. 1989, Ph.D. thesis, University of California, Los Angeles
———. 1990, A&A, 238, 191
Mihalas, D. 1978, Stellar Atmospheres (San Francisco: Freeman)
Natta, A., & Beckwith, S. 1986, A&A, 158, 310
Nomoto, K., Thielemann, F.-K., & Yokoi, K. 1984, ApJ, 286, 644
Olson, G. L. 1982, ApJ, 255, 267
Pauldrach, A. W. A. 1987, A&A, 183, 295
Pauldrach, A. W. A., Puls, J., & Kudritzki, R. P. 1986, A&A, 164, 86
Puls, J. 1987, A&A, 184, 227
Puls, J., & Hummer, D. G. 1988, A&A, 191, 87
Rybicki, G. B. 1970, in NBS Spec. Publ., No. 332, Spectrum Formation in Stars with Steady-State Extended Atmospheres, ed. H. G. Groth & P. Wellmann (Washington, D.C: GPO), 87
Rybicki, G. B., & Hummer, D. G. 1978, ApJ, 219, 654 (RH)
Schmidt, B. P. 1992, private communication
Sobolev, V. V. 1947, Moving Envelopes of Stars (Leningrad: Leningrad State Univ.) (English trans.: S. Gaposchkin [Cambridge: Harvard Univ. Press, 1960])
Thielemann, F.-K., Nomoto, K., & Yokoi, K. 1986, A&A, 158, 17
Wegner, G., & McMahan, R. K. 1987, AJ, 93, 287
Wheeler, J. C., & Harkness, R. P. 1990, Rep. Prog. Phys., 53, 1467